

1
2
3 **Surface Modification of a MXene by an Aminosilane Coupling Agent**
4
5

6 Hossein Riazi, Mark Anayee, Kanit Hantanasirisakul, Ahmad Arabi Shamsabadi,
7 Babak Anasori, Yury Gogotsi, and Masoud Soroush*
8
9

10 H. Riazi, Dr. A. A. Shamsabadi, Prof. M. Soroush

11 Department of Chemical and Biological Engineering, Drexel University, Philadelphia,
12 Pennsylvania, 19104, United States

13 M. Anayee, K. Hantanasirisakul, Dr. B. Anasori, Prof. Y. Gogotsi

14 A.J. Drexel Nanomaterials Institute and Department of Material Science and Engineering, Drexel
15 University, Philadelphia, Pennsylvania, 19104, United States

16
17 **SECOND REVISED VERSION**
18

19 January 14, 2019
20

21 Submitted for publication in Advanced Materials Interfaces
22
23
24

25 Keywords: $Ti_3C_2T_x$, MXene, Surface Functionalization, Aminosilane, Self-Assembly
26

27 *Corresponding author. ms1@drexel.edu; 1-(215)-895-1710
28
29

30 **Abstract**

31 MXenes, 2D transition metal carbides and/or nitrides, possess surface termination groups
32 such as hydroxyl, oxygen, and fluorine, which are available for surface functionalization. Their
33 surface chemistry is critical in many applications. This article reports amine-functionalization of
34 $Ti_3C_2T_x$ MXene surface with 3-(2-aminoethylamino)-propyltrimethoxysilane (AEAPTMS).
35 Characterization techniques such as X-ray photoelectron spectroscopy verify the success of the
36 surface functionalization and confirm that the silane coupling agent bonds to $Ti_3C_2T_x$ surface both
37 physically and chemically. The functionalization changes the MXene surface charge from -35 mV
38 to $+25$ mV at neutral pH, which allows for in-situ preparation of self-assembled films. Further,
39 surface charge measurements of the functionalized MXene at different pH show that the
40 functionalized MXene has an isoelectric point at a pH around 10.7, and the highest reported surface
41 charge of $+62$ mV at a pH of 2.58. Furthermore, the existence of a mixture of different orientations
42 of AEAPTMS and simultaneous presence of protonated and free amine groups on the surface of
43 $Ti_3C_2T_x$ are demonstrated. The availability of free amine groups on the surface potentially permits
44 the fabrication of crosslinked electrically-conductive MXene/epoxy composites, dye adsorbents,
45 high-performance membranes, and drug carriers. Surface modifications of this type are applicable
46 to many other MXenes.

47 **1. Introduction**

48 MXenes are a large family of two-dimensional (2D) transition metal carbides and/or
49 nitrides derived primarily through the selective etching of the A-group element layers in layered
50 ternary transition metal carbides and/or nitrides (MAX phases) with hydrofluoric acid (HF) or in-
51 situ generation of HF using lithium fluoride and hydrochloric acid.^[1-3] The general formula of
52 MAX is $M_{n+1}AX_n$ and that of MXene is $M_{n+1}X_nT_x$, where 'M' is an early transition metal, 'A' is a
53 group 13 or 14 element such as Al and Si, 'X' is C and/or N, and 'T' represents surface functional
54 groups such as O, OH, F, and Cl.^[4] The integer 'n' is between 1 and 3. After etching, the multilayer
55 MXene nanosheets can be delaminated into single-layer flakes by manual shaking or sonication.^[5]
56 $Ti_3C_2T_x$ was the first MXene discovered and remains the most widely studied MXene primarily
57 due to the well-established methods for synthesis and material handling.^[6] The negative surface
58 charge of -39.4 mV is reported for fresh $Ti_3C_2T_x$ which originates from the negatively charged
59 surface terminations.^[7] MXenes retain their negative surface charge in the wide pH range of 4-12,
60 resulting in high colloidal stability that enables facile solution processing and surface
61 modifications.^[8] Similar to other 2D nanomaterials, MXenes usually appear in the form of stacked
62 sheets and their properties strongly depend on their morphology – stacked bundles versus
63 individual sheets – and the type of chemical species present between the 2D flakes and on the
64 surface.^[9-10]

65 Silane coupling agents are capable of forming durable bonds between organic and
66 inorganic materials. Silane molecules have zero to three alkoxy groups connected to a central
67 silicon atom and a fourth alkyl chain with varying organofunctional groups such as amine,
68 diamine, methacrylate, epoxy, vinyl, chloro, and phenyl. The alkoxy groups can be converted to
69 silanol groups through hydrolysis reaction by the addition of water separately, from moisture in
70 the air, or from water adsorbed on the surface of nanomaterials. Typically, hydrolysis reactions

71 can be catalyzed by the addition of acids or bases to the reaction medium, whereas several coupling
72 agents, like amine-bearing ones, have shown self-catalysis properties.^[11] It is hypothesized that the
73 generated silanol groups can form covalent bonds with hydroxyl groups available on the surface
74 of nanomaterials through a dehydration reaction. Inadvertently, side reactions like
75 homocondensation of the coupling agents may also occur which causes the formation of a highly
76 crosslinked polymer through the formation of Si-O-Si bonds.

77 To date, there have been only a few studies on surface functionalization of MXenes with
78 silane coupling agents.^[12-16] Zhang *et al.* functionalized $Ti_3C_2T_x$ with 3-(methacryloxy)
79 propyltrimethoxysilane (MPS) and subsequently grafted sulfonated polyelectrolyte brushes on the
80 surface by a surface-initiated precipitation polymerization technique.^[13] They incorporated the
81 surface functionalized MXene into a poly(ether ether ketone) matrix to fabricate proton conducting
82 membranes. The surface of $Ti_3C_2T_x$ was also functionalized with 1H, 1H, 2H, 2H–
83 perfluorodecyltrimethoxysilane by Zhao *et al.* and with 1H, 1H, 2H, 2H–
84 perfluorooctyltriethoxysilane by Cao *et al.* to develop superhydrophobic MXene for solar
85 desalination systems and self-cleaning coatings, respectively.^[14, 16] Lim *et al.* also used alkylsilane
86 coupling agents to increase surface hydrophobicity of $Ti_3C_2T_x$ to make it dispersible in non-polar
87 solvents like hexane.^[15] Therefore, silane coupling agents with various organofunctional groups
88 enable a wide variety of applications.

89 With respect to silane coupling agents possessing amine functional groups, Hao *et al.* used
90 (3-aminopropyl)triethoxysilane (APTES) to functionalize the surface of $Ti_3C_2T_x$ for thin-film
91 membranes in polyacrylonitrile (PAN) or polydimethylsiloxane (PDMS) matrix, which showed
92 strong enhancement in flux and selectivity for alcohol based solvents.^[17] Kumar *et al.* also used
93 APTES to functionalize the surface of $Ti_3C_2T_x$ for detection of cancer biomarkers.^[12] Furthermore,
94 amine functional groups can improve MXene stability and enable MXenes to undergo various

95 reactions such as epoxide ring-opening, ureidation, and salt formation with sulfonic and carboxylic
96 acids.^[18-19] The previous studies found MXene-aminosilane nanocomposites to be promising
97 potential candidates for various applications. However, none of them investigated the different
98 types of interactions that exist between the silane coupling agents and MXene, the effects of the
99 interactions on the surface charge at different pH values, or thermal decomposition behavior of the
100 functionalized MXenes. Furthermore, as surface functionalization of MXenes should be conducted
101 under mild acidic conditions and inert gas bubbling, to prevent MXene oxidation,^[6, 20] there is a
102 need for developing a reliable protocol for the functionalization.

103 To the best of our knowledge, so far only two studies have been published on functionalized
104 MXenes with a positive surface charge. One altered the surface charge using a metal ion and the
105 other using an aminosilane coupling agent.^[19,21] However, these studies did not investigate: (a)
106 how surface charge varies with the suspension pH; (b) where the isoelectric point is located, which
107 is important in the layer-by-layer film assembly process; (c) the effect of aminosilane
108 functionalization on thermal behavior of the MXene flakes; (d) the effect of thermal annealing on
109 the interlayer distance of the functionalized MXene flakes; and (e) the chemistry of amine groups
110 after their placement on the MXene surface.

111 We grafted 3-(2-aminoethylamino)propyltrimethoxysilane (AEAPTMS) on the surface of
112 $Ti_3C_2T_x$. Proton nuclear magnetic resonance (1H NMR) spectroscopy was carried out to confirm
113 the hydrolysis of the AEAPTMS. Fourier-transform infrared spectroscopy (FTIR) was used to
114 confirm the reaction of $Ti_3C_2T_x$ surface hydroxyl groups. X-ray photoelectron spectroscopy (XPS)
115 was utilized to verify the presence of different functional groups on the MXene surface and
116 distinguish the different modes of interactions. Energy-dispersive X-ray spectroscopy (EDS) was
117 performed to confirm the homogenous distribution of AEAPTMS over the surface.
118 Thermogravimetric analysis (TGA) and evolved gas mass spectroscopy (MS) were used to

119 investigate the strength of the interactions between AEAPTMS and $\text{Ti}_3\text{C}_2\text{T}_x$ and confirm that both
120 physically adsorbed and covalently bonded AEAPTMS are available on the surface. Zeta-potential
121 measurements were performed in a wide pH range to confirm the change in the surface charge
122 from negative to positive upon the surface functionalization and find the isoelectric point of the
123 functionalized MXene. Scanning electron microscopy (SEM) and transmission electron
124 microscopy (TEM) were carried out to evaluate the morphology of MXene flakes before and after
125 the surface functionalization. Furthermore, X-Ray diffraction (XRD) results showed that the
126 surface functionalization increases the inter-layer distance between the MXene flakes. Finally, to
127 demonstrate applicability of the functionalized MXene, self-assembled MXene films were
128 prepared by mixing the negatively and positively charged $\text{Ti}_3\text{C}_2\text{T}_x$ flakes.

129

130 **2. Results and Discussion**

131 The chemical reaction between AEAPTMS and the hydroxyl groups of $\text{Ti}_3\text{C}_2\text{T}_x$ is shown
132 schematically in Figure 1. Our characterization results indicate that AEAPTMS molecules interact
133 with $\text{Ti}_3\text{C}_2\text{T}_x$ through two modes; the silanol group ends leading to covalent bonding and the amine
134 group ends leading to electrostatic interaction.

135 Although some primary or secondary amines in the presence of water are able to catalyze
136 the detachment of already bonded coupling agents from the surface of nanomaterials, it has been
137 shown that AEAPTMS does not suffer from this problem in aqueous media.^[22] In addition, the
138 chance of a reaction between hydrolyzed methoxy groups of AEAPTMS and hydroxyl groups on
139 the surface of $\text{Ti}_3\text{C}_2\text{T}_x$ is higher for this aminosilane coupling agent compared with its
140 counterparts.^[22] In addition to the kind of aminosilane, proper reaction conditions are needed for
141 the completion of the chemical reaction (high grafting efficiency), as discussed below.

142 The temperature, pH, and water/ethanol ratio are important parameters that dictate the
143 efficacy of the surface functionalization reaction. The parameters were chosen based on the
144 recommended values.^[23-24] A reaction medium pH of 3.5 was found to ensure a high grafting
145 efficiency and prevent silane coupling agents from homocondensation.^[25-26] The reaction was
146 carried out at room temperature, as dissolved oxygen in water may accelerate $Ti_3C_2T_x$ degradation
147 at higher temperatures.^[6] A low ratio of water to ethanol (10/90 wt.%) was used to prevent the
148 detachment of the bonded molecules from the surface of $Ti_3C_2T_x$ after functionalization. In fact,
149 water is only needed to convert the methoxy groups of the silane coupling agent to hydroxyl
150 groups through the hydrolysis reaction.^[27]

151 **Figure 1.**

152 Hydrolysis of AEAPTMS releases methoxy groups in the form of methanol as the reaction
153 side product. Hydrogen bonds between the silanol groups and the –OH surface termination groups
154 of $Ti_3C_2T_x$ are then formed, followed by the formation of covalent bonds between $Ti_3C_2T_x$ and
155 hydrolyzed AEAPTMS (Figure S1C in Supporting Information (SI)). In addition, electrostatic
156 attractions between negatively charged surface of $Ti_3C_2T_x$ and the positively charged protonated
157 amine groups of the silane coupling agent may exist. In this case, non-hydrolyzed/hydrolyzed
158 methoxy groups are left non-bonded to the surface (Figure S1A and S1B).

159 We performed 1H NMR spectroscopy to confirm the successful hydrolysis of AEAPTMS.
160 The spectra of AEAPTMS in D_2O as well as a mixture of pristine $Ti_3C_2T_x$ and AEAPTMS in D_2O ,
161 in both neutral and acidic media, are presented in Figure 2. Regarding 1H NMR results of
162 AEAPTMS, we expected to see eight different peaks as the molecule has eight different kinds of
163 hydrogen (Figure S2). However, the number of peaks is lower than what is expected (Figure 2A).
164 This may be due to overlapping of some peaks with each other, the hydrogen bonding between the
165 species in the system or other solvent effects.^[28-31] Figure 2A shows a sharp peak around 3.3 ppm,

166 which can be attributed to the hydrogens in the methoxy groups (3.3–3.6 ppm).^[32] These are the
167 hydrogen that are labeled as type 1 in Figure S2. Other small peaks highlighted by vertical arrows
168 I, II, and III in Figure 2A possibly represent other kinds of hydrogens in the silane coupling agent
169 as the system just consists of AEAPTMS, D₂O, and the solvent residue.^[32-33] The hydrogens
170 corresponding to each of these arrows are discussed in Figure S2. When acetic acid was added to
171 this system (Figure 2B), a new peak at 3.34 ppm appeared, which verifies the hydrolysis of the
172 methoxy groups and the release of methanol as the side product.^[33] The same phenomenon was
173 observed when the silane coupling agent was mixed with pristine Ti₃C₂T_x and the MXene-acetic
174 acid systems (Figures 2C and 2D). These results show that the presence of Ti₃C₂T_x does not
175 negatively interfere in the hydrolysis reaction. As methoxy groups participated in the hydrolysis
176 reaction, we then expect that the surface functionalization can proceed by a covalent bond
177 formation between the surface of Ti₃C₂T_x and AEAPTMS.

178

Figure 2.

179 FTIR spectroscopy on the pristine and AEAPTMS-Ti₃C₂T_x (Figure 3A) revealed two new
180 peaks at 2924 and 2855 cm⁻¹ (inset) that appeared after Ti₃C₂T_x surface functionalization, which
181 are attributed to symmetric and asymmetric vibrations of the C–H bonds in the alkyl chain of
182 AEAPTMS, respectively. Moreover, the peak highlighted by an arrow around 1580 cm⁻¹ can be
183 ascribed to the bending mode of N–H bond of the primary amine.^[34-35] The broad peak around
184 3500 cm⁻¹ can originate from both surface -OH terminations as well as possibly entrapped water
185 molecules. Thus, the disappearance of this peak in the FTIR spectrum of AEAPTMS-Ti₃C₂T_x can
186 be an indication of successful functionalization of Ti₃C₂T_x with AEAPTMS through the reaction
187 of –OH MXene surface termination groups with silanol groups of AEAPTMS, which results in the
188 conversion of Ti–O–H into Ti–O–Si bonds.^[15] Another possibility is that incorporation of large

189 organic molecules on the surface breaks the network of hydrogen bonding between nearby
190 hydroxyl groups which is the cause of broad hydroxyl group peak in FTIR spectra.^[36]

191 To confirm the presence and protonation state of amine groups on the surface of the
192 AEAPTMS-Ti₃C₂T_x, the N1s high resolution XPS spectrum was obtained (Figure 3B, Tables S1
193 & S2). The spectrum was deconvoluted into two peaks corresponding to free and protonated
194 amines at binding energies of 400.2 eV and 402.0 eV, respectively.^[37-39] The ratio of free to
195 protonated amines was found to be ~1.72:1 based on the ratio of the Relative Sensitive Factor
196 (RSF) adjusted integral area of the two deconvoluted N1s region peaks. Furthermore, the small
197 peak at ~397.2 eV is attributed to nitrogen coordinated with a metal which in this case is Ti, thereby
198 forming Ti–N covalent bonds.^[40] Similar to the condensation reaction between the silanol groups
199 and the hydroxyl surface terminations forming Ti–O–Si bonds, condensation reaction between the
200 amine groups and the hydroxyl surface terminations leads to release of water and formation of Ti–
201 N bonding. Such Ti–N bonding and condensation reaction have been reported in Ti₃C₂T_x MXene
202 coated on (3-aminopropyl)triethoxy silane modified PET by Park *et al.*^[41] However, due to the low
203 concentration of this specie and thereby low intensity and signal-to-noise ratio, it was not included
204 in the XPS deconvolution analysis. The Si2p high resolution spectrum (Figure S3) was fit with a
205 single peak at 102.7 eV corresponding to Si–O–Si linkages between neighboring AEAPTMS
206 molecules arising from polycondensation reactions.^[42] Moreover, this same peak can also be
207 attributed to Si–O–Ti linkages which are presumed to exist due to the disappearance of the
208 hydroxyl stretching mode from FTIR and the observance of two types of nitrogen functional
209 groups in the N1s XPS spectrum which likely originate from the two possible orientations of the
210 AEAPTMS on the surface of Ti₃C₂T_x.

211

Figure 3.

212 Scanning electron microscopy (SEM) is used widely to observe the sheet-like structure of
213 MXenes.^[43,2] Here, we conducted SEM on the cross-section of AEAPTMS-Ti₃C₂T_x and found that
214 the layered structure of the pristine MXene stays intact even after functionalization reaction. TEM
215 results also confirmed that MXene keeps its layered structure after the surface functionalization
216 (Figure S4). We also performed EDS to map the distributions of titanium, fluorine, oxygen, carbon,
217 silicon, and nitrogen in the AEAPTMS-Ti₃C₂T_x structure and its surface (Figures S5). The first
218 four elements are inherently available in the structure of Ti₃C₂T_x, while the presence of silicon and
219 nitrogen atoms are indicative of the surface functionalization (Figure S6). The nitrogen and silicon
220 are likely to originate from the covalently bonded or the physically adsorbed AEAPTMS
221 molecules as washing process with ethanol was repeated three times after the reaction to remove
222 unreacted silane coupling agents.^[44] The results show that the AEAPTMS molecules uniformly
223 distribute on the MXene surface.

224 To evaluate the different types and strength of bonding between AEAPTMS and Ti₃C₂T_x,
225 TGA and MS of pristine and AEAPTMS-Ti₃C₂T_x were performed and presented in Figure 4. The
226 thermogram of pristine MXene indicates the dehydration of the material from 25 °C up to ~300
227 °C,^[43] which correlates to water (m/z=18) curve in the MS shown in Figure 4B. High temperatures
228 are required to dehydrate free-standing MXene films due to the intercalation of water in small
229 interlayer spacing of ~10 Å. Decomposition of pristine Ti₃C₂T_x starts ~750 °C, resulting in CO
230 release as shown by the m/z=28 curve in the Figure 4B.^[45-46] Decomposition of Ti₃C₂T_x also results
231 in the evolution of CO₂ and HF gases along with the transformation of the scaffold into titanium
232 carbide (TiC).^[47] The AEAPTMS-Ti₃C₂T_x decomposes at the same temperature regime indicating
233 that the decomposition behavior of Ti₃C₂T_x scaffold is not affected by the silane functionalization
234 process.

235 In contrast, thermogram of the AEAPTMS- $\text{Ti}_3\text{C}_2\text{T}_x$ exhibits three distinct weight loss steps
236 in the 25–500 °C range. The first step with a maximum rate of change at ~95 °C corresponds to the
237 desorption of water and ethanol from AEAPTMS- $\text{Ti}_3\text{C}_2\text{T}_x$. The shoulder at ~175 °C in the (m/z=18
238 and 17) spectra can be attributed to the dehydration of the intercalated water molecules. The boiling
239 point of pure AEAPTMS is ~260 °C which corresponds well with the second TGA weight loss
240 step having a maximum rate of change at ~260 °C.^[48] The sharp increase in the methane and amine
241 anion (m/z = 16) and ammonia (m/z = 17) release starting at ~240 °C with a maximum at ~315 °C
242 agree well with the evolution of physisorbed AEAPTMS. The slight increase in this temperature
243 from 260 °C to 315 °C can also be ascribed to the intercalation of the AEAPTMS in the interlayer
244 spacing of $\text{Ti}_3\text{C}_2\text{T}_x$ and to electrostatic interactions between NH_3^+ of AEAPTMS and –OH surface
245 termination groups of the $\text{Ti}_3\text{C}_2\text{T}_x$. The third weight loss step in the thermogram can be related to
246 the loss of AEAPTMS covalently bonded to $\text{Ti}_3\text{C}_2\text{T}_x$ as indicated by the onset and maximum in
247 the derivative thermogravimetry (DTG) curve at ~350 °C and ~450 °C, respectively. Moreover, the
248 peaks in the methane, amine (m/z = 16) and ammonia (m/z = 17) MS curves at ~400 °C and the
249 peak in the CO (m/z = 28) MS curve at ~438 °C further corroborate the decomposition of covalently
250 bonded AEAPTMS.

251 Overall, the TGA results here are consistent with reports on GLYMO- TiO_2 ,^[49] APTES-
252 SiO_2 ,^[50] and other surface functionalized nanoparticles,^[51-52] in which three weight loss steps exist
253 in the 25–500 °C range. Yamazaki *et al.* attributed the three weight loss steps to physisorbed
254 monomeric silanes, physisorbed polycondensated silanes, and chemisorbed silanes.^[50] Salon *et*
255 *al.* indicated that compared to silane coupling agents with other functional groups, those based on
256 amino groups exhibit fast polycondensation kinetics, hence the expected large second weight loss
257 step.^[53] Overall, the exact control of each of those types of interactions is out of the scope of this

258 research; However, the presence of chemisorbed silane species on the $\text{Ti}_3\text{C}_2\text{T}_x$ surface expands the
259 applications of this functionalized MXene.

260 **Figure 4.**

261 Another indication of the presence of free amine groups on AEAPTMS- $\text{Ti}_3\text{C}_2\text{T}_x$ surface is
262 the change in its surface charge. Zeta potential measurements were conducted on the pristine and
263 functionalized MXene dispersions in a pH range of ~ 2.5 to ~ 12 , within pristine $\text{Ti}_3\text{C}_2\text{T}_x$ MXene
264 colloid is stable. $\text{Ti}_3\text{C}_2\text{T}_x$ MXene in strongly basic medium ($\text{pH} > 12$) degrades quickly due to
265 attack by hydroxyl ions. On the other hand, $\text{Ti}_3\text{C}_2\text{T}_x$ MXene dispersions in strongly acidic medium
266 ($\text{pH} < 2.5$) agglomerate and settle out of solution due to high concentration of H^+ ion, which leads
267 to self-assembly and structuring of the sheets.^[54] Unlike pristine $\text{Ti}_3\text{C}_2\text{T}_x$ which has a negative
268 surface charge in the pH range of ~ 2.5 to ~ 12 , AEAPTMS- $\text{Ti}_3\text{C}_2\text{T}_x$ showed a positive surface
269 charge of more than 20 mV in a wide pH window from ~ 2.5 to ~ 10 enabling it to participate in
270 further surface functionalization reactions in neutral media (Figure 5A). The AEAPTMS- $\text{Ti}_3\text{C}_2\text{T}_x$
271 also keeps its pH responsiveness as free amine groups, similar to hydroxyl groups, are capable of
272 gaining or losing H^+ upon change in the medium pH.^[34] As the pH increases, the concentration of
273 H^+ ions decreases and the concentration of OH^- ions increases, leading to deprotonation of the
274 ammonium group and a decrease in the overall positive charge of the particle. Likewise, as the pH
275 decreases, protonation of the amine group occurs which increases the overall positive charge of
276 the particle.^[55-57] The AEAPTMS- $\text{Ti}_3\text{C}_2\text{T}_x$ has an isoelectric point between pH 10.58 and 10.8 as
277 indicated by the surface charges of +1.73 mV and -12.34 mV, respectively. Furthermore, the
278 surface charge of +62 mV at pH = 2.58 is the largest positive charge reported for MXenes to date.

279 From the application point of view, the synthesis of a positively charged $\text{Ti}_3\text{C}_2\text{T}_x$ allows
280 for its self-assembly with the pristine MXene, which inherently possesses a negative surface
281 charge.^[58] Figure 5B represents the pristine MXene, AEAPTMS- $\text{Ti}_3\text{C}_2\text{T}_x$, and the layer obtained

282 from their assembly. Xie *et al.* used layer-by-layer assembled films made from positively charged
283 carbon nanotubes and pristine MXene to fabricate electrodes for sodium-based batteries.^[59] In their
284 research, the carbon nanotube acted as a spacer between MXene sheets. Here, similarly,
285 electrostatic interactions make it possible to form a film while the restacking of the MXene
286 nanosheets can be prohibited due to the grafted aminosilane molecules, which potentially play the
287 role of a spacer.

288 **Figure 5.**

289 XRD measurements on free-standing pristine and functionalized $Ti_3C_2T_x$ films both
290 annealed at 250 °C showed an increase in the interlayer spacing from 11.7 Å to 13.2 Å upon surface
291 functionalization based on shift of the (002) peak from 7.55° to 6.67° (Figure S7). Similarly, for
292 the samples at room temperature and the ones annealed at 60 °C, functionalized MXene showed a
293 peak at lower angles (larger interlayer spacing) compared with the corresponding pristine MXene.
294 Furthermore, the broadening of the (002) peak after functionalization and heat treatment at 250 °C
295 is due to less regular spacing between the layers after removal of intercalated solvent and
296 physically adsorbed aminosilane, which leave behind only chemically bonded silanes. The
297 increase in the interlayer spacing can still be seen through the tail towards lower 2-theta values.

298 Overall, the presence of free amine groups on the surface of AEAPTMS- $Ti_3C_2T_x$ that are
299 available for subsequent reactions opens the door for a wide variety of applications. For example,
300 functionalized MXenes can act as curing agents for epoxy resins and allow the development of
301 electrically conductive composites.^[60] In addition, they can play the role of substrates for surface-
302 initiated atom transfer radical polymerization, electrodes for energy-storage devices and metal ion
303 absorber.^[61-64] The results presented in this article point to the potential of MXenes for self-
304 assembly, which permits bottom-up manufacturing of nano-devices. Ensembles of nanoparticles
305 made by self-assembly are used in nanoscale thermometer, data storage devices, catalysis

306 recovery, magnetic data storage, delivery of biologically active species, electrochemical
307 biosensors, etc.^[65]

308 **3. Conclusion**

309 The surface of $Ti_3C_2T_x$ was functionalized with AEAPTMS. Hydroxyl groups on the
310 surface of the pristine $Ti_3C_2T_x$ provide suitable sites for the aminosilane grafting. By doing so, we
311 were able to change the surface charge of $Ti_3C_2T_x$ from highly negative to +62 mV at pH = 2.58,
312 which is the largest positive zeta potential value reported for MXenes. Our results showed that the
313 AEAPTMS- $Ti_3C_2T_x$ is still a pH responsive nanomaterial due to the presence of amine groups on
314 its surface, which are capable of adsorbing or desorbing protons upon change in pH. The
315 simultaneous presence of protonated and free amine groups on the surface of AEAPTMS- $Ti_3C_2T_x$
316 was confirmed by XPS. Homogenous distributions of silicon and nitrogen elements were also
317 observed by EDS. All characterization results together confirmed the presence of amine groups on
318 the surface of the AEAPTMS- $Ti_3C_2T_x$. This functionalization method should be applicable to other
319 MXene structures and compositions. The amine-functionalization expands the range of
320 applications of MXenes in many areas such as antibacterial coatings, fuel cells, surface-initiated
321 polymerization, dye adsorbents, and drug delivery systems.

322 **4. Experimental**

323 **4.1. Materials**

324 Ethanol [anhydrous $\geq 99.9\%$] was purchased from Electron Microscopy Science Co.
325 Sodium hydroxide (NaOH) [$\geq 97\%$] was purchased from Merck Co., and glacial acetic acid
326 (CH_3COOH) [100%] was supplied by BDH Co. AEAPTMS [$\geq 96\%$] and deuterium oxide (D_2O)
327 with 99.8 % atom D were purchased from Alfa Aesar. Hydrochloric acid (HCl) [41-58 %], and
328 lithium fluoride (LiF) [99.98%] were purchased from Fisher Scientific Co. Ti_3AlC_2 was obtained

329 from Carbon Ukraine (Kyiv, Ukraine). The polypropylene membrane, 3501 Coated PP, was
330 purchased from Celgard LLC Co. (Charlotte, NC, US). All chemicals were used as they were
331 received (without any purification).

332 **4.2. $Ti_3C_2T_x$ MXene Synthesis**

333 Ti_3AlC_2 MAX phase was selectively etched to form $Ti_3C_2T_x$ by adding Ti_3AlC_2 (2 g, < 75
334 μm particle size) to an etchant solution containing LiF (3.2 g) and HCl (9 M, 40 mL) over the
335 course of ~5 minutes to avoid overheating due to the exothermic nature of the reaction. The
336 suspension was stirred at 300 rpm with a polytetrafluoroethylene (PTFE) coated stir bar at room
337 temperature for 24 hours in a loosely capped polyethylene terephthalate (PET) bottle. The resulting
338 suspension was washed 5 times via centrifugation at 3500 rpm for 5 minutes with DI water in a
339 175 mL centrifuge tube until the pH reached ~6. Following washing, the suspension was bath-
340 sonicated for 1 hour at 100 W using a bath sonicator (2510 Branson). Next, the suspension was
341 centrifuged at 3500 rpm for 5 minutes to remove multilayer MXene and unetched MAX. The
342 supernatant was then centrifuged at 10,000 rpm for 2 hours to concentrate the solution.

343 **4.3. $Ti_3C_2T_x$ Functionalization Procedure**

344 Surface functionalization of $Ti_3C_2T_x$ was carried out in a water/ethanol mixture (10/90
345 wt.%) in order to provide enough amount of water for AEAPTMS hydrolysis reaction. The
346 reaction was performed at room temperature and its medium was stirred (600 rpm) for 8 hours
347 under nitrogen bubbling. First, ethanol was added to an aqueous suspension of $Ti_3C_2T_x$, and acetic
348 acid was then added to decrease the pH of the reaction medium to 3.5. To obtain the concentration
349 of $Ti_3C_2T_x$ suspensions, a given volume of each suspension was first vacuum filtered and the mass
350 of the corresponding freestanding film was then measured. A part of the total ethanol used for the
351 reaction, was reserved for preparing silane in ethanol solution. To ensure the occurrence of the

352 reaction between OH terminations of $\text{Ti}_3\text{C}_2\text{T}_x$ and AEAPTMS, a silane to $\text{Ti}_3\text{C}_2\text{T}_x$ mass ratio of
353 2:1 was used. Next, the solution of the silane coupling agent in ethanol was added dropwise to the
354 reaction medium during the first 2 hours of the reaction. After completion of the reaction, the
355 suspension was washed three times with ethanol by centrifugation at 3500 rpm to remove
356 unreacted silane coupling agents from AEAPTMS- $\text{Ti}_3\text{C}_2\text{T}_x$ nanosheets. The final suspension was
357 vacuum-filtered on polypropylene membranes and the obtained free-standing films were
358 subsequently dried in vacuum oven at 60 °C for 24 hours. To get $\text{Ti}_3\text{C}_2\text{T}_x$ powder, the final
359 suspension was cast in a Teflon petri dish and kept under vacuum to evaporate its liquid medium.

360 **4.4. Characterization**

361 Fourier-transform infrared (FTIR) spectroscopy on pristine and AEAPTMS- $\text{Ti}_3\text{C}_2\text{T}_x$
362 powders (Thermo Fisher Nicolet iS50 FTIR Spectrometer, USA) was carried out in attenuated
363 total reflectance (ATR) mode with a diamond crystal in the range of 4000 - 400 cm^{-1} with a step
364 size of 0.5 cm^{-1} and 32 measurement cycles.

365 Zeta potential measurements (NanoBrook ZetaPALS, Brookhaven Instrument, USA) were
366 performed on the AEAPTMS- $\text{Ti}_3\text{C}_2\text{T}_x$ powder re-dispersed in water by sonication for 30 minutes
367 as well as on the pristine MXene. NaOH and CH_3COOH aqueous solutions were used to adjust
368 the pH of the system. Each test was repeated at least three times and the average values along with
369 their uncertainty range were reported.

370 Thermogravimetric analysis and evolved gas mass spectrometry were carried out on the
371 pristine MXene and AEAPTMS- $\text{Ti}_3\text{C}_2\text{T}_x$ free-standing films using SDT 650 TGA coupled with
372 Discovery MS (TA Instruments, USA). The tests were conducted from room temperature to 1000
373 °C with a heating rate of 10 °C · min^{-1} under a flowing helium atmosphere at 100 $\text{mL} \cdot \text{min}^{-1}$.

374 Prior to the test, the furnace was purged with $100 \text{ mL} \cdot \text{min}^{-1}$ of helium for 1 h to remove residual
375 air.

376 X-ray photoelectron spectroscopy (XPS) was conducted on the free-standing films using
377 PHI VersaProbe 5000 instrument (Physical Electronics, USA) with a $200 \mu\text{m}$ and 50 W
378 monochromatic Al-K_α (1486.6 eV) X-ray source. Charge neutralization was accomplished through
379 a dual beam setup using low energy Ar^+ ions and low energy electrons at $1 \text{ eV}/200 \mu\text{A}$. High-
380 resolution F1s , O1s , Ti2p , N1s , C1s , Si2p and Fermi energy region spectra were collected using a
381 pass energy of 23.5 eV and an energy resolution of 0.05 eV. Survey spectrum was collected using
382 a pass energy of 117 eV and an energy resolution of 0.5 eV. No binding energy scale correction
383 was applied as the samples were not charged during the analysis. Quantification and peak fitting
384 were conducted using CasaXPS V2.3.19.

385 ^1H NMR spectroscopy (500 MHz Varian Unity Inova NMR, USA) was performed by
386 dissolving AEAPTMS in D_2O or dispersing a mixture of $\text{Ti}_3\text{C}_2\text{T}_x$ powder and AEAPTMS in D_2O .
387 The suspension of $\text{Ti}_3\text{C}_2\text{T}_x$ in D_2O was prepared by bath-sonication (Branson 1200) for 30 minutes
388 to ensure fine dispersion of the nanomaterial in D_2O . pH of the system was adjusted by adding
389 CH_3COOH .

390 Scanning electron microscopy (SEM) and Energy-dispersive X-ray spectroscopy (EDS)
391 were carried out, respectively, using Zeiss Supra 50 VP, USA, and an EDS detector (Oxford
392 Instruments, Ultim Max) mounted on it. Samples were prepared by drop-casting of the
393 AEAPTMS- $\text{Ti}_3\text{C}_2\text{T}_x$ suspension on a microscope glass to obtain powdered material. The samples
394 were then mounted on carbon tape and sputter-coated with platinum.

395 Transmission electron microscopy (TEM) was carried out using a JEOL JEM2100 microscope.
396 Samples were prepared by drop-casting of the pristine $\text{Ti}_3\text{C}_2\text{T}_x$ and AEAPTMS- $\text{Ti}_3\text{C}_2\text{T}_x$

397 suspensions on TEM grids. The girds were then placed in a desiccator connected to a vacuum
398 pump to assure that the samples were dried completely.

399 X-ray diffraction (XRD) (Rigaku Miniflex 600 diffractometer) was conducted on free-
400 standing films using a monochromatic Cu K-alpha X-ray source. Survey scans were conducted
401 from 3° to 65° with a step size of 0.03° at $5^\circ \cdot \text{min}^{-1}$. High resolution scans were conducted from
402 3° to 10° with a step size of 0.01° at $0.5^\circ \cdot \text{min}^{-1}$.

403

404 **Supporting Information**

405 Supporting Information is available from the Wiley Online Library or from the author.

406

407 **Conflict of Interest**

408 Authors declare no financial/commercial conflict of interest.

409

410 **Acknowledgment**

411 Hossein Riazi and Ahmad A. Shamsabadi were partially supported by the U.S. National
412 Science Foundation under Grant No. CBET-1804285. Any opinions, findings, and conclusions or
413 recommendations expressed in this material are those of the authors and do not necessarily reflect
414 the views of the National Science Foundation.

415 **References**

- 416 [1] B. Anasori, Y. Gogotsi, *2D Metal Carbides and Nitrides (MXenes)*. Springer, **2019**.
- 417 [2] B. Anasori, M. R. Lukatskaya, Y. Gogotsi, *Nat. Rev. Mater.* **2017**, 2 (2), 16098.
- 418 [3] A. A. Shamsabadi, M. Gh, B. Anasori, M. Soroush, *ACS Sustain. Chem. Eng.* **2018**, 6 (12),
419 16586-16596.
- 420 [4] M. Naguib, V. N. Mochalin, M. W. Barsoum, Y. Gogotsi, *Adv. Mater.* **2014**, 26 (7), 992-
421 1005.
- 422 [5] M. Malaki, A. Maleki, R. S. Varma, *J. Mater. Chem. A* **2019**, 7 (18), 10843-10857.

423 [6] C. J. Zhang, S. Pinilla, N. McEvoy, C. P. Cullen, B. Anasori, E. Long, S.-H. Park, A. s.
424 Seral-Ascaso, A. Shmeliov, D. Krishnan, *Chem. Mater.* **2017**, 29 (11), 4848-4856.

425 [7] C. E. Ren, K. B. Hatzell, M. Alhabeb, Z. Ling, K. A. Mahmoud, Y. Gogotsi, *J. Phys.*
426 *Chem. Lett.* **2015**, 6 (20), 4026-4031.

427 [8] M. Naguib, R. R. Unocic, B. L. Armstrong, J. Nanda, *Dalton T.* **2015**, 44 (20), 9353-9358.

428 [9] Z. Zhou, J. Liu, X. Zhang, D. Tian, Z. Zhan, C. Lu, *Adv. Mater. Interfaces.* **2019**, 6 (6),
429 1802040.

430 [10] M. Lu, W. Han, H. Li, H. Li, B. Zhang, W. Zhang, W. Zheng, *Adv. Mater. Interfaces.* **2019**,
431 6 (8), 1900160.

432 [11] M.-C. B. Salon, M. Abdelmouleh, S. Boufi, M. N. Belgacem, A. Gandini, *J. Colloid Interf.*
433 *Sci.* **2005**, 289 (1), 249-261.

434 [12] S. Kumar, Y. Lei, N. H. Alshareef, M. Quevedo-Lopez, K. N. Salama, *Biosens.*
435 *Bioelectron.* **2018**, 121, 243-249.

436 [13] J. Zhang, Y. Liu, Z. Lv, T. Zhao, P. Li, Y. Sun, J. Wang, *Solid State Ionics* **2017**, 310, 100-
437 111.

438 [14] J. Zhao, Y. Yang, C. Yang, Y. Tian, Y. Han, J. Liu, X. Yin, W. Que, *J. Mater. Chem. A*
439 **2018**, 6 (33), 16196-16204.

440 [15] S. Lim, H. Park, J. Yang, C. Kwak, J. Lee, *Colloid. Surface. A.* **2019**, 579, 123648.

441 [16] W.-T. Cao, W. Feng, Y.-Y. Jiang, C. Ma, Z.-F. Zhou, M.-G. Ma, Y. Chen, F. Chen, *Mater.*
442 *Horiz.* **2019**, 6 (5), 1057-1065.

443 [17] L. Hao, H. Zhang, X. Wu, J. Zhang, J. Wang, Y. Li, *Compos. Part A-App. S.* **2017**, 100,
444 139-149.

445 [18] E. P. Plueddemann, *Silane coupling agents*, Springer Science+Business Media, LLC, New
446 York, **1991**

447 [19] J. Ji, L. Zhao, Y. Shen, S. Liu, Y. Zhang, *FlatChem* **2019**, 100128.

448 [20] S. Seyedin, E. R. S. Yanza, J. M. Razal, *J. Mater. Chem. A* **2017**, 5 (46), 24076-24082.

449 [21] Z. Huang, L. Biwu, L. Juewen, *Langmuir* **2019**, 35(30), 9858-9866.

450 [22] M. Zhu, M. Z. Lerum, W. Chen, *Langmuir* **2011**, 28 (1), 416-423.

451 [23] M.-C. B. Salon, M. N. Belgacem, *Colloid. Surface. A.* **2010**, 366 (1-3), 147-154.

452 [24] O. Paquet, M.-C. B. Salon, E. Zeno, M. N. Belgacem, *Mater. Sci. Eng., C* **2012**, 32 (3),
453 487-493.

454 [25] R. Bel-Hassen, S. Boufi, M.-C. B. Salon, M. Abdelmouleh, M. N. Belgacem, *J. Appl.*
455 *Polym. Sci.* **2008**, 108 (3), 1958-1968.

456 [26] H. Ishida, J. L. Koenig, *J. Colloid Interf. Sci.* **1978**, 64 (3), 555-564.

457 [27] X. Liu, J. Xing, Y. Guan, G. Shan, H. Liu, *Colloid. Surface. A.* **2004**, 238 (1-3), 127-131.

458 [28] Y. Tataurova, M. J. Sealy, R. G. Larsen, S. C. Larsen, *J. Phys. Chem. Lett.* **2012**, 3 (3), 425-
459 429.

460 [29] L. Yao, A. Grishaev, G. Cornilescu, A. Bax, *J. Am. Chem. Soc.* **2010**, 132 (31), 10866-
461 10875.

462 [30] J. W. Akitt, B. E. Mann, *NMR and Chemistry: An introduction to modern NMR*
463 *spectroscopy*. Crc Press, **2000**

464 [31] P. Needham, *Stud. Hist. Philos. Sci.* **2013**, 44 (1), 51-65.

465 [32] S. Sasaki, *Handbook of proton-NMR spectra and data*. Academic Press, **1985**

466 [33] G. R. Fulmer, A. J. Miller, N. H. Sherden, H. E. Gottlieb, A. Nudelman, B. M. Stoltz, J. E.
467 Bercaw, K. I. Goldberg, *Organometallics* **2010**, 29 (9), 2176-2179.

468 [34] J. Zhao, M. Milanova, M. M. Warmoeskerken, V. Dutschk, *Colloid. Surface. A* **2012**, *413*,
469 273-279.

470 [35] X. Wang, W. Xing, P. Zhang, L. Song, H. Yang, Y. Hu, *Compos. Sci. Technol.* **2012**, *72*
471 (6), 737-743.

472 [36] T. Kondo, *Cellulose* **1997**, *4* (4), 281-292.

473 [37] J. Pels, F. Kapteijn, J. Moulijn, Q. Zhu, K. Thomas, *Carbon* **1995**, *33* (11), 1641-1653.

474 [38] R. Jansen, H. Van Bekkum, *Carbon* **1995**, *33* (8), 1021-1027.

475 [39] R. Liu, W. Li, *ACS Omega* **2018**, *3* (3), 2609-2617.

476 [40] D. Jaeger, J. Patscheider, *Sur. Sci. Spectra* **2013**, *20* (1), 1-8.

477 [41] T.H. Park, S. Yu, M. Koo, H. Kim, E.H. Kim, J.E. Park, B. Ok, B. Kim, S.H. Noh, C. Park,
478 E. Kim, C.M. Koo, C. Park, *ACS Nano* **2019**, *13*, 6835-6844.

479 [42] P. C. Ma, J.-K. Kim, B. Z. Tang, *Carbon* **2006**, *44* (15), 3232-3238.

480 [43] J. L. Hart, K. Hantanasirisakul, A. C. Lang, B. Anasori, D. Pinto, Y. Pivak, J. T. van Omme,
481 S. J. May, Y. Gogotsi, M. L. Taheri, *Nat. Commun.* **2019**, *10* (1), 522.

482 [44] F. Ahangaran, A. Hassanzadeh, S. Nouri, *Int. Nano Lett.* **2013**, *3* (1), 23.

483 [45] J. Zhu, E. Ha, G. Zhao, Y. Zhou, D. Huang, G. Yue, L. Hu, N. Sun, Y. Wang, L. Y. S. Lee,
484 *Coord. Chem. Rev.* **2017**, *352*, 306-327.

485 [46] Y. Cao, Q. Deng, Z. Liu, D. Shen, T. Wang, Q. Huang, S. Du, N. Jiang, C.-T. Lin, J. Yu,
486 *RSC Adv.* **2017**, *7* (33), 20494-20501.

487 [47] Z. Li, L. Wang, D. Sun, Y. Zhang, B. Liu, Q. Hu, A. Zhou, *Mater. Sci. Eng., B* **2015**, *191*,
488 33-40.

489 [48] M. Ash, *Handbook of fillers, extenders, and diluents*. Synapse Info Resources, Inc., **2007**.

490 [49] W. Que, Y. Zhou, Y. Lam, Y. Chan, C. Kam, *J. Sol-Gel Sci. Technol.* **2001**, *20* (2), 187-
491 195.

492 [50] R. Yamazaki, N. Karyu, M. Noda, S. Fujii, Y. Nakamura, *J. Appl. Polym. Sci.* **2016**, *133*
493 (14).

494 [51] A. Shanmugharaj, J. Bae, K. Y. Lee, W. H. Noh, S. H. Lee, S. H. Ryu, *Compos. Sci.*
495 *Technol.* **2007**, *67* (9), 1813-1822.

496 [52] Z. Luan, J. A. Fournier, J. B. Wooten, D. E. Miser, *Microporous Mesoporous Mater.* **2005**,
497 *83* (1-3), 150-158.

498 [53] M.-C. B. Salon, P.-A. Bayle, M. Abdelmouleh, S. Boufi, M. N. Belgacem, *Colloid.*
499 *Surface. A* **2008**, *312* (2-3), 83-91.

500 [54] S. J. Kim, J. Choi, K. Maleski, K. Hantanasirisakul, H. T. Jung, Y. Gogotsi, C. W. Ahn,
501 *ACS Appl. Mater. Inter.* **2019**, *11*(35), 32320-32327.

502 [55] L. Liu, Z. Guo, Z. Huang, J. Zhuang, W. Yang, *Sci. Rep.* **2016**, *6*, 22029.

503 [56] S.H. Huang, D.H. Chen. *J. Hazard. Mater.* **2009**, *163*(1), 174-179.

504 [57] X. He, K. Wang, D. Li, W. Tan, C. He, S. Huang, B. Liu, X. Lin, X. Chen, *J. Disper. Sci.*
505 *Technol.* **2003**, *24*(3-4), 633-640.

506 [58] J. Yang, W. Bao, P. Jaumaux, S. Zhang, C. Wang, G. Wang, *Adv. Mater. Interfaces* **2019**,
507 *6* (8), 1802004.

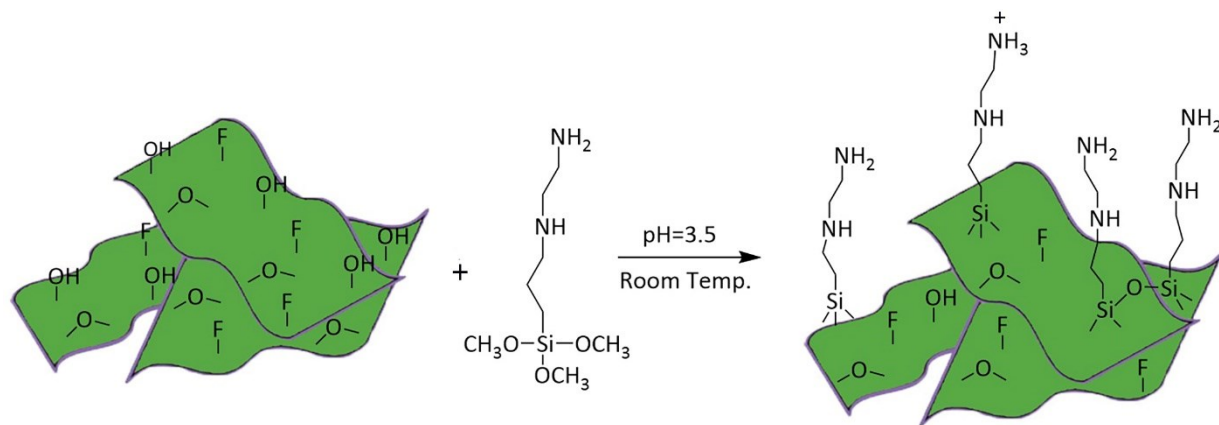
508 [59] X. Xie, M.-Q. Zhao, B. Anasori, K. Maleski, C. E. Ren, J. Li, B. W. Byles, E.
509 Pomerantseva, G. Wang, Y. Gogotsi, *Nano Energy* **2016**, *26*, 513-523.

510 [60] S. Wang, Z. Liang, T. Liu, B. Wang, C. Zhang, *Nanotechnology* **2006**, *17* (6), 1551.

511 [61] A. VahidMohammadi, J. Moncada, H. Chen, E. Kayali, J. Orangi, C. A. Carrero, M.
512 Beidaghi, *J. Mater. Chem. A* **2018**, *6* (44), 22123-22133.

513 [62] A. Ali, K. Hantanasirisakul, A. Abdala, P. Urbankowski, M.-Q. Zhao, B. Anasori, Y.
 514 Gogotsi, B. Aïssa, K. A. Mahmoud, *Langmuir* **2018**, *34* (38), 11325-11334.
 515 [63] S. B. Ambade, R. B. Ambade, W. Eom, S. H. Noh, S. H. Kim, T. H. Han, *Adv. Mater.*
 516 *Interfaces* **2018**, *5* (24), 1801361.
 517 [64] L. Fu, Z. Yan, Q. Zhao, H. Yang, *Adv. Mater. Interfaces* **2018**, *5* (23).
 518 [65] Z. Nie, A. Petukhova, E. Kumacheva, *Nat. Nanotechnol.* **2010**, *5*(1), 15.

519



520 **Figure 1.** Schematic representation of the pristine $\text{Ti}_3\text{C}_2\text{T}_x$ flakes reacting with the 3-(2-
 521 aminoethylamino) propyltrimethoxysilane coupling agent.

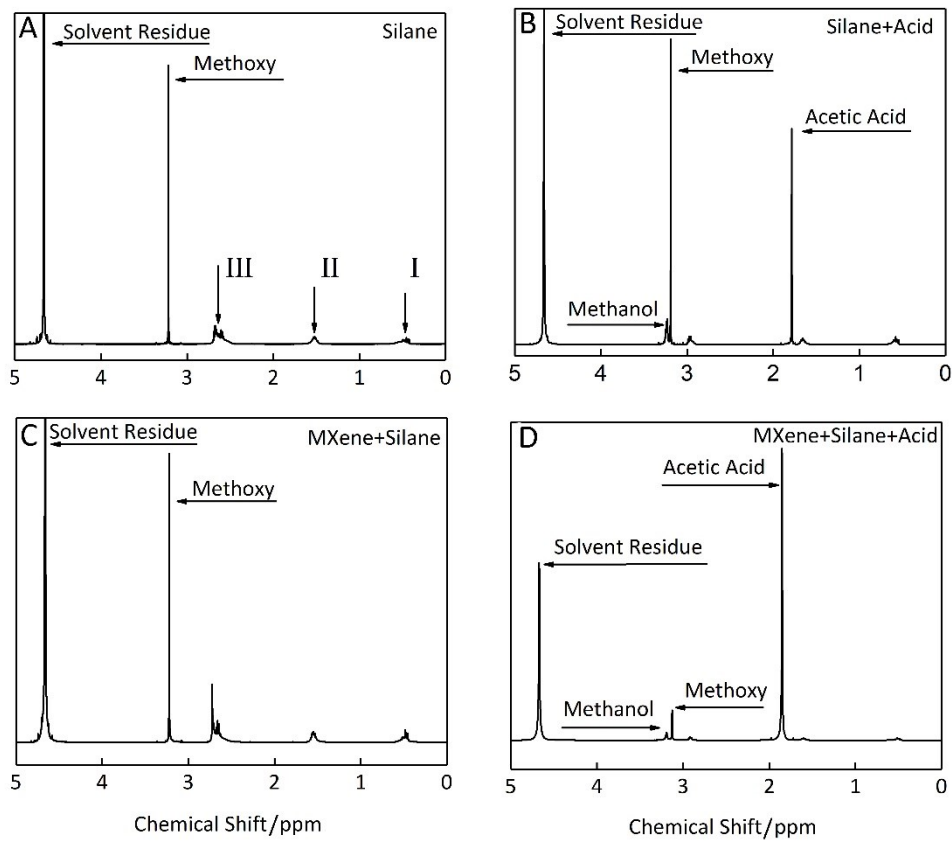
522

523

524

525

526



527

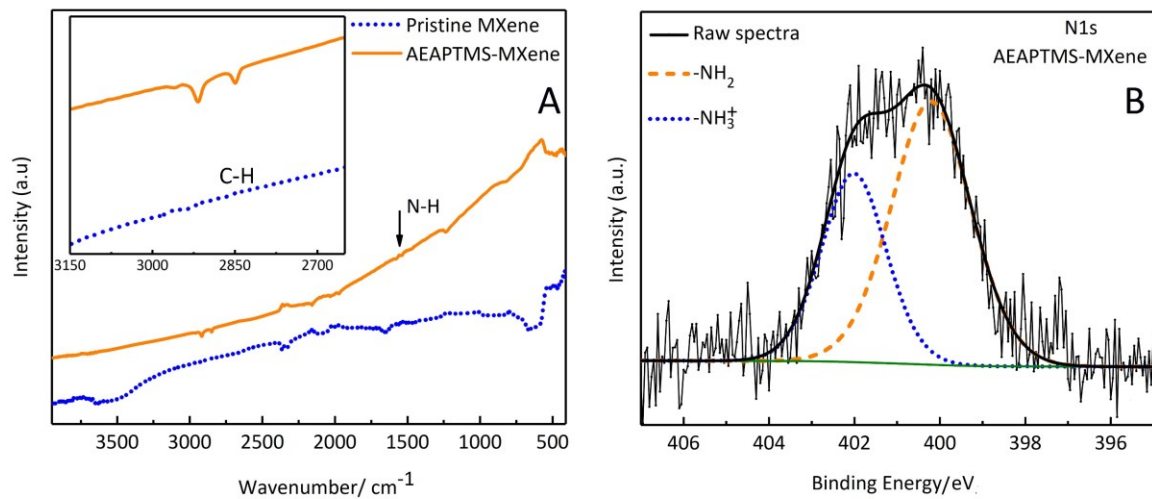
528 **Figure 2.** ^1H NMR spectra of the silane coupling agent in (A) neutral and (B) acidic media, and a
 529 mixture of MXene/silane coupling agent in (C) neutral and (D) acidic media.

530

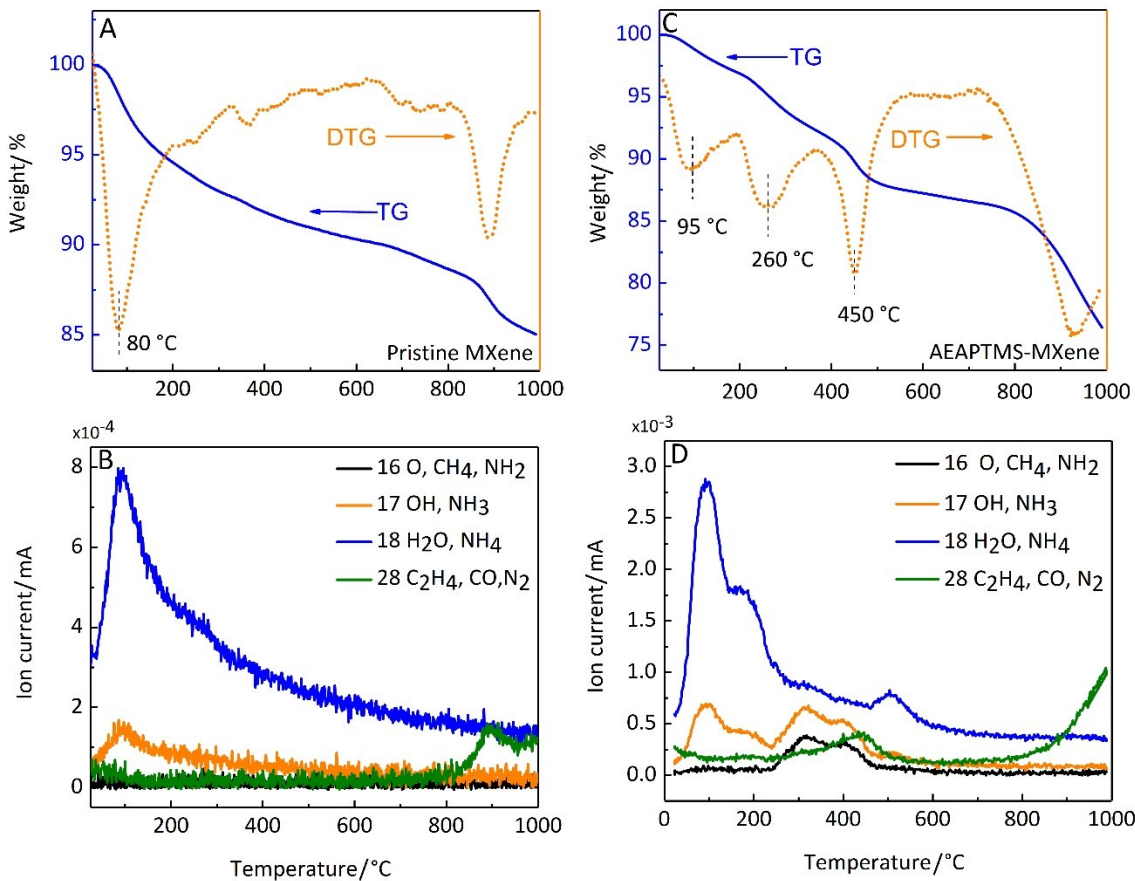
531

532

533



536 **Figure 1.** (A) FTIR spectra of the pristine $\text{Ti}_3\text{C}_2\text{T}_x$ and the AEAPTMS- $\text{Ti}_3\text{C}_2\text{T}_x$. (B) High-
 537 resolution N1s XPS spectrum deconvoluted into two peaks for free (400.2 eV) and protonated
 538 amines (402.0 eV).



543

544

545 **Figure 4.** (A) TGA thermogram of pristine $\text{Ti}_3\text{C}_2\text{T}_x$ showing one sharp weight loss peak at 25-500
 546 °C, (B) mass spectroscopy of pristine $\text{Ti}_3\text{C}_2\text{T}_x$ showing release of H_2O , OH , and CO , (C) TGA
 547 thermogram of AEAPTMS- $\text{Ti}_3\text{C}_2\text{T}_x$ showing three different weight loss steps in the 25-500 °C
 548 range, and (D) mass spectroscopy of AEAPTMS- $\text{Ti}_3\text{C}_2\text{T}_x$ showing the release of O , NH_2 , OH ,
 549 H_2O , and CO .

550

551

552

553

554

555

556

557

